energies

Article

Multi-Objective Parameter Optimized Design of Self-Oscillating Cavitation Jet Nozzles

Tengwei Wang [1], Guohui Li [2], Mengbin Song [1], Yuanyuan Zhao [3], Wei Xu [4], Fujian Zhao [5] and Xiuli Wang [5,*]

1 LEO Group Hunan Pump Co., Ltd., Jiuhua Demonstration Zone, Xiangtan 212013, China; wangtengwei@leopump.com (T.W.); songmb@leogroup.cn (M.S.)
2 GongQing Institute of Science and Technology, Jiujiang 332020, China; lghgqkj@163.com
3 School of the Environment and Safety Engineering, Jiangsu University, Zhenjiang 212013, China; zyy-michelle@163.com
4 School of Energy and Power Engineering, Jiangsu University, Zhenjiang 212013, China; xuwei791837@hotmail.com
5 Research Center of Fluid Machinery Engineering and Technology, Zhenjiang 212013, China; zfj@stmail.ujs.edu.cn
* Correspondence: ujslthb@163.com

Abstract: Self-oscillating cavitation jet technology has become a research hotspot of scholars in various fields. However, existing research lacks a summary of the rules of the influence of various factors on the cavitation performance, such that efficient and stable extensive engineering applications are impossible to achieve. This paper aims at optimizing the design of the self-oscillating cavitation jet nozzle (SOCJN) as the objective; this is carried out by the experimental design, optimal Latin hypercube method, and response surface method in (design of experiment) DOE methods on the basis of the ISIGHT optimization method. In addition, taking the vapor volume fraction and cavitation number as a research objective, the obtained optimal structural parameters of the nozzles are applied under the condition of clear water to establish the function mapping relationship between the external geometric characteristics and the vapor volume fraction and cavitation number; then, this is compared with the experiment. The results indicate that the second-order response surface approximate model is suitable for the SOCJN and there is an error smaller than 8% between the approximate model results and the calculated results of the nozzle response. When the diameter of the upper nozzle is D_1 = 4.7 mm, the ratio of the upper nozzle's diameter to the lower's diameter (D_1/D_2) is 2.6 and the ratio of the chamber length to the chamber diameter (L/D) is 0.63; pulse jets from the SOCJN have the best pitting effect on the sample at the monitoring point when the convergence angle of collision wall α is 120°. When the structural parameters of the nozzle are optimal structural parameters, the cavitation performance is the best at the initial pressure of 4.8 MPa. This research provides a reference for the optimized design of the SOCJN for industrial applications.

Keywords: self-oscillating; cavitation jet nozzle; design optimization; structural parameters; cavitation number; vapor volume fraction

Citation: Wang, T.; Li, G.; Song, M.; Zhao, Y.; Xu, W.; Zhao, F.; Wang, X. Multi-Objective Parameter Optimized Design of Self-Oscillating Cavitation Jet Nozzles. *Energies* **2023**, *16*, 6737. https://doi.org/10.3390/en16186737

Academic Editor: Marco Marengo

Received: 26 July 2023
Revised: 8 September 2023
Accepted: 18 September 2023
Published: 21 September 2023

1. Introduction

In the process of industrial development, a large amount of industrial organic wastewater being generated every day is harmful to human health and the environment. Currently, the ways for treating industrial wastewater mainly include physical, chemical, and biological methods. However, these methods cannot fulfill the treatment requirements of organic wastewater well [1,2]. In recent years, because of its simple structure [3,4], outstanding degradation effect, and zero secondary pollution, the hydrodynamic cavitation degradation technology has gradually become a hot spot in the research of organic wastewater treatment [5,6]. Hydrodynamic cavitation can be produced by changes in flow and pressure and its generation is usually based on a specific structure. The self-oscillating pulse jets formed by the self-oscillating nozzle [7,8] have a strong cavitation effect in this type of structure [9]. The research on self-oscillating jet nozzles has an important academic and market value.

Currently known parameters that have a greater impact on the cavitation performance of the SOCJN include the inlet diameter, outlet diameter, chamber diameter, chamber length, collision wall convergence angle, and inlet pressure [10]. The inlet and outlet diameters and chamber length of the nozzle are very important to the cavitation performance. The change to the collision wall convergence angle directly influences the distribution of jet flow field performance, especially the distribution of the pressure field in the nozzle; the low-pressure area is a key factor for the formation and development of cavitation [11]. The inlet pressure is the input source of the overall jet energy, which directly influences jet power. Moreover, inlet pressure has a great influence on the cavitation ability and erosion effect of jets [12]. Li et al. [13] analyzed and deduced the natural frequency of the organ pipe's resonant chamber in accordance with the principles of transient flow and hydroacoustic, obtained the design mode, and found that the diameter and length of the resonant chamber were key factors affecting the resonance of resonant fluid through experiments, thus summarizing the design mode of the SOCJN on the basis of the organ pipe's resonant chamber model. Liu et al. [14] researched the aeration treatment of the chamber structure; analyzed the diameters, positions, and number of different aeration holes; and proposed a solution of using a structure with front and rear chambers distributed symmetrically, which had a high degree of cavitation.

Researching the influence of the structure parameters of the SOCJN on the internal cavitation jet flow field, Qi et al. [15] applied a series of methods to establish a two-chamber self-oscillating cavitation nozzle for numerical simulation, obtaining the influence law of the incoming flow Reynolds number and the ratio of the front chamber's length and diameter to the rear chamber on the cavitation jets. Yuan et al. [16] took the chamber angle, chamber diameter, chamber length, and outlet diameter as design variables; they then took impact peak value and impact pulsation amplitude as target variables and the order of influence of each factor was obtained. Wang et al. [17] and Makhsuda et al. [18] studied the flow field characteristics of the Helmholtz self-oscillating cavitation device based on numerical simulation and concluded that when outlet pressure is constant, the cavitation performance can be enhanced by increasing inlet pressure and the structure with the cone collision wall has the most obvious effect.

In this paper, aiming at optimizing the design of the SOCJN, numerical simulation is carried out for inlet pressure and the structural parameters of the nozzle to evaluate the cavitation ability of the jet flow field and the influence weight of each parameter on the nozzle, which provides a reference for the optimized design of the SOCJN for treating industrial wastewater.

2. Numerical Calculation Model

2.1. Model Construction

2.1.1. Geometric Model

The principles of the SOCJN are shown in Figure 1, in which the left is the nozzle and the right is the submerged fluid domain. After the fluid enters the nozzle from the inlet of the left nozzle, self-oscillation is triggered in the self-oscillating chamber to change it from continuous flowing fluid to pulsed jets. The peak velocity of the pulsed jets is raised according to the self-oscillating characteristics [19] and the cavitation effect of the fluid is strengthened in the process. The pulsed jets leaving the nozzle are mixed with a large number of cavitation bubbles, which enter the submerged fluid area subsequently. Due to the sudden increase in pressure, a large number of cavitation bubbles will collapse to generate energy that provides power, so as to achieve cavitation degradation [20].

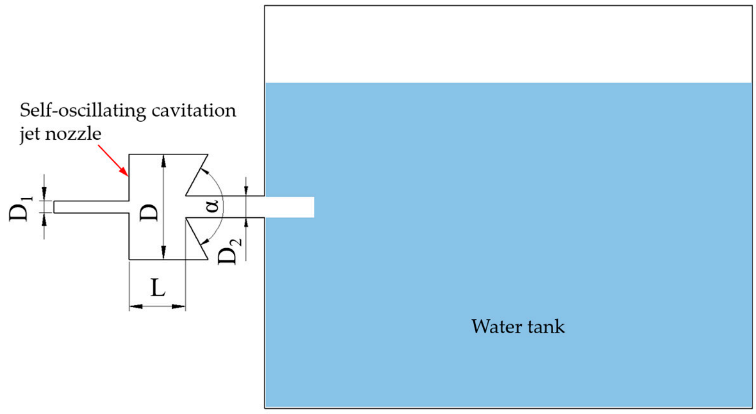

Figure 1. The structure schematic diagram of the SOCJN.

The main structure of the nozzle is as follows. The inlet diameter of the jet nozzle is D_1. The outlet diameter of the nozzle is D_2 and the diameter of the chamber is D. The length of the chamber is L. The collision angle is α and the dimensionless structural parameters of the nozzle shall meet the value ranges shown in Table 1.

Table 1. Values ranges of the dimensionless parameters of the SOCJN.

Dimensionless Parameters	D_2/D_1	L/D	D/D_2	α
Value ranges	1.84~2.67	0.53~0.84	5~6.9	120°

2.1.2. Model Selection

A highly complex cavitation flow phenomenon happens in the self-oscillating cavitation jet. In this paper, because the nozzle has a large intermediate flow velocity and more shear flow inside the chamber, there is a higher requirement of capturing tiny cavitation bubbles. Therefore, the VOF model is taken as the multiphase flow model, which is more applicable for simulating the jet under the condition of limited computing resources. In this paper, the large number of tiny cavitation bubbles generated in the chamber raises the difficulty of converging during the calculation so we adopt the Zwart-Gerber-Belamri cavitation model in order to improve the convergence and reduce the computational cost [21]. In addition, the k-ε turbulence model is selected for simulation in this paper.

2.2. Boundary Condition Setting and Mesh Independence Verification

The fluent finite volume element method is adopted to carry out numerical simulations of the cavitation flow in the SOCJN. The boundary conditions are as follows. The inlet pressure is set as the inlet boundary condition and the 1 atm outlet pressure is set as the outlet boundary condition. In addition, it is assumed that the liquid phase on the wall satisfies the condition of no-slip and the wall function is used to deal with the near-wall area. A total of 290,000, 500,000, 830,000, and 1.4 million structured grids are selected for inspection. The same model is applied for steady-state simulation and the average flow velocity and average relative static pressure at the outlet of the nozzle are taken as reference. The results are shown in Figure 2. When the grid number is less than 500,000, the fluctuation of resulting data is violent and the simulation results are less reliable at this time. When the number of grids is greater than 500,000, the results of simulating the average flow velocity at the outlet of the nozzle are influenced slightly and the data point is basically stable at about 83.3 m/s. However, the data also fluctuate slightly when the number of grids is greater than 1.2 million; this may be caused by the large number of grids and uneven local encryption but the small influence can be ignored. As shown in Figure 3, the change in the cavitation number at the outlet from the center to the pipe wall can be clearly displayed by comparing the cavitation numbers on the outlet sections. The data comparison of different numbers indicates that the grid number has a slight influence on the distribution of the cavitation number of the outlet section. The data results clearly reflect that the cavitation number tends to be larger from the center to the wall. The comparison between the static pressure with the vapor volume fraction and the cavitation number indicates that the grid number has little effect on the latter two parameters. Both of them could well reflect the collapse of the fluid containing cavitation bubbles after leaving the nozzle and entering the water tank. Considering the limited amount of computation, this paper adopts 500,000 to 600,000 grids.

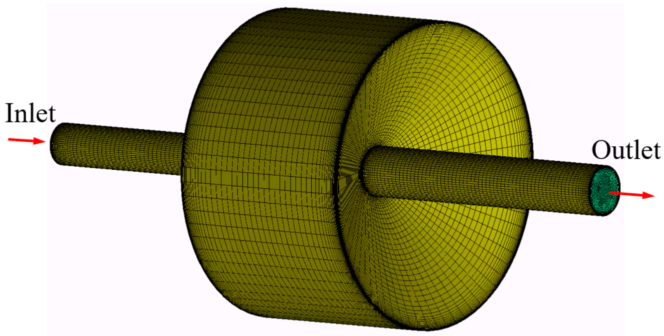

Figure 2. Grid schematic diagram of the SOCJN for numerical simulation.

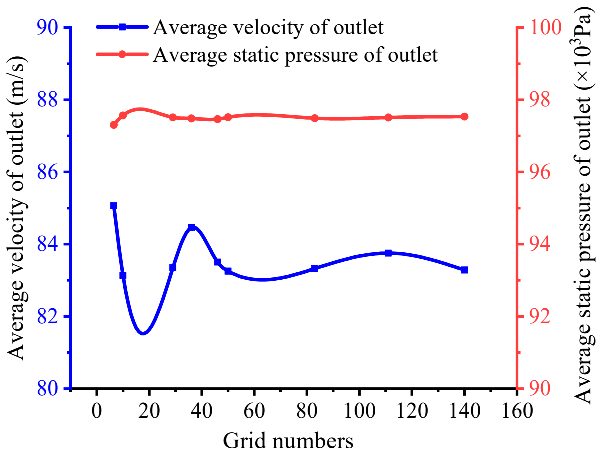

Figure 3. Cavitation number at the nozzle outlet section with different grid numbers.

2.3. Optimization Design Method

This paper mainly adopts DOE analysis methods in a multidisciplinary optimized design, taking the geometrical parameters of the SOCJN as the factors in the DOE, the geometrical parameter values as the level values of the factors, and the results obtained on the basis of the different level designs of each factor as the response values to obtain the optimal parameters of the SOCJN under the given conditions through the response surface method. In total, 120 experiments are carried out for each design variable using the Eu-Latin hypercube design method.

2.3.1. Response Surface Methodology Design

The structural parameters and working parameters of the nozzle directly affect the cavitation performance. The design variables and value ranges selected in this paper are shown in Table 2. The specific simulation results are shown in Table A1.

Table 2. Values ranges of the design variables of the SOCJN.

Variables	D_1 (mm)	C_{D21} (%)	C_{LD} (%)	C_{DD2} (%)	P_{in} (MPa)
Value ranges	(4, 5)	(1.84, 2.67)	(0.53, 0.84)	(5, 6.9)	(4, 5)
Values	4	2	0.68	5.94	4

Among them, the design variable D_1 is the inlet diameter of the SOCJN. C_{D21} is the ratio of the outlet diameter D_2 to the inlet diameter D_1 of the nozzle. C_{LD} is the ratio of the chamber length L to the chamber diameter D_2. C_{DD2} is the ratio of the chamber diameter D to the outlet diameter D_2. P_{in} is the inlet pressure of the nozzle. The output variables include the cavitation number (σ) and the vapor volume fraction (VOF). As an output variable, the σ is used to describe the cavitation phenomenon in hydraulics. The σ is a dimensionless parameter. If σ_1 represented the critical cavitation number at which cavitation just appears or disappears, there is no cavitation when $\sigma > \sigma_1$. When $\sigma < \sigma_1$, it is a stage of cavitation occurrence. The smaller the value is, the more serious the cavitation degree is. The VOF is used to measure the vapor volume contained in the nozzle, which reflects the cavitation degree. The response surface method [22] is used to optimize the SOCJN and 120 groups of sample points are obtained by using the experimental design method, 80 of which are used for establishing approximate models; 40 groups of sample points are used for error analysis.

2.3.2. Response Surface Approximation Model

ISIGHT is applied to establish a multivariate quadratic regression model according to the sample points and the model is expressed by a coefficient table. The coefficients of the response cavitation number (σ) and the VOF are shown in Tables 3 and 4.

The first column in the coefficient table reflects the main effect of each term in the polynomial model on the response. As can be seen from Tables 3 and 4, there are not only the main effects of the linear terms C_{D21}, C_{LD}, C_{DD2}, D_1, and P_{in} but also the main effects of the second-order terms of the linear terms and the interaction effects of the linear terms in the polynomial model. The scaled column in the table reflects the model coefficients after the input variables are normalized to [−1, +1] and fitted by the least square method, which can more fairly reflect the contribution of each input variable to the response.

Table 3. Quadratic regression model coefficient table of the cavitation number.

	Coefficients	**Scaled**	**Normalized**
constant	82.4505		
C_{D21}	−26.7853	0.1325	4.2597
C_{LD}	−9.9129	0.3658	11.7604
C_{DD2}	−2.3058	0.0227	0.7298
D_1	−10.2506	0.1104	3.5500
P_{in}	-4.3385×10^{-8}	−0.0051	−0.1642
$C_{D21}{}^2$	2.2025	0.4460	14.3407
$C_{LD}{}^2$	0.2893	0.2893	9.3027
$C_{DD2}{}^2$	−1.1500	−0.0460	−1.4790
$D_1{}^2$	0.2425	0.0606	1.9495
Pin^2	-6.3×10^{-15}	−0.0251	−0.8061
C_{D21}-C_{LD}	1.5059	0.6777	21.7891
C_{D21}-C_{DD2}	0.2028	0.0183	0.5869
C_{D21}-D_1	1.7887	0.4025	12.9401
C_{D21}-P_{in}	-1.9271×10^{-8}	−0.0173	−0.5577
C_{LD}-C_{DD2}	0.4484	0.0897	2.8837
C_{LD}-D_1	0.6815	0.3407	10.9555
C_{LD}-P_{in}	1.2723×10^{-8}	0.0255	0.8182
C_{DD2}-D_1	0.2019	0.0202	0.6489
C_{DD2}-P_{in}	-8.5629×10^{-9}	−0.0034	−0.1101
D_1-P_{in}	1.1433×10^{-8}	0.0114	0.3676

Table 4. Quadratic regression model coefficient table of the vapor volume fraction.

	Coefficients	Scaled	Normalized
constant	−20.0317		
C_{D21}	8.7278	−0.0690	−5.824
C_{LD}	2.0508	−0.2336	−19.724
C_{DD2}	−1.7765	−0.0077	−0.6525
D_1	2.8451	−0.0890	−7.519
P_{in}	2.5093×10^{-9}	0.0002	0.0146
$CD_{21}{}^2$	−0.8838	−0.1790	−15.11
$C_{LD}{}^2$	−0.0481	−0.0481	−4.064
$C_{DD2}{}^2$	0.2969	0.0119	1.003
$D_1{}^2$	−0.1151	−0.0288	−2.429
$P_{in}{}^2$	-3.1×10^{-15}	−0.0123	−1.038
C_{D21}-C_{LD}	−0.4236	−0.1906	−16.10
C_{D21}-C_{DD2}	0.2660	0.0239	2.022
C_{D21}-D_1	−0.5581	−0.1256	−10.60
C_{D21}-P_{in}	-1.2488×10^{-8}	−0.0112	−0.9490
C_{LD}-C_{DD2}	−0.0708	−0.0142	−1.196
C_{LD}-D_1	−0.1527	−0.0764	−6.449
C_{LD}-P_{in}	-5.644×10^{-9}	−0.0113	−0.9532
C_{DD2}-D_1	0.2225	0.0223	1.879
C_{DD2}-P_{in}	4.913×10^{-8}	0.0197	1.659
D_1-P_{in}	9.685×10^{-9}	0.0097	0.8178

2.3.3. Approximate Model Variance Analysis

Variance analysis is applied to test the significance of the difference between two or more sample means. The data obtained from the research fluctuate due to the influence of various factors. According to the analysis of variance, it is believed that the total variance of the response comes from two parts, including the polynomial model and uncontrollable random factors, namely, the fitting error. Tables 5 and 6 are the tables of the variance analysis results of the nozzle's cavitation number and VOF, respectively.

Table 5. Analysis of variance of the cavitation number.

	DF	SS	V	F	R^2	P
Model	20	16.94	0.85	32.01	0.87	0.0001
Error	97	2.56	0.03	-	-	-
Total	117	19.50	-	-	-	-

Table 6. Vapor volume fraction variance analysis results.

	DF	SS	V	F	R^2	P
Model	20	3.52	0.18	28.44	0.85	0.0001
Error	97	0.60	0.006	-	-	-
Total	117	4.12	-		-	-

The R-squared coefficients of the regression models for the cavitation number and VOF are 0.8687 and 0.8543, indicating that the two regression models had a high fitting degree.

2.4. Experimental Scheme

A cavitation degradation test is carried out on the SOCJN researched in this paper in order to verify the reliability of the optimized design scheme. Figure 4 shows a schematic diagram of a degradation test bench for the SOCJN. The structural parameters of the nozzle are shown in Table 7.

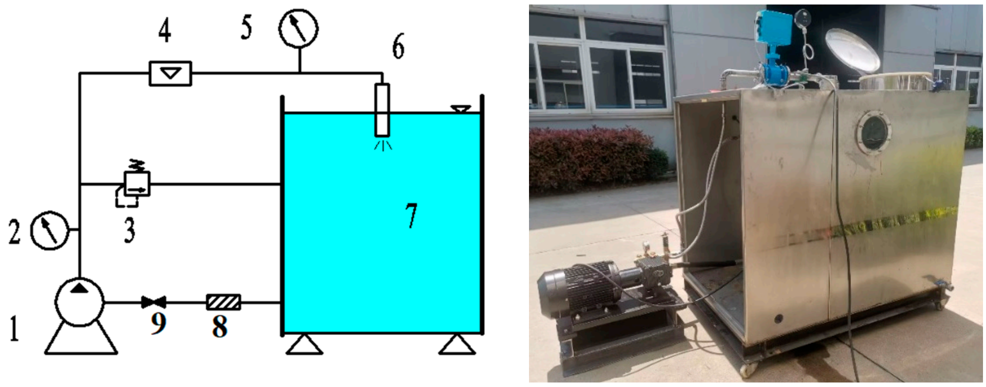

(**a**) Schematic diagram (**b**) Test platform

Figure 4. Schematic diagram of the test platform (1: plunger pump, 2: pump pressure gauge, 3: pressure-regulating relief valve, 4: electromagnetic flowmeter, 5: pressure gauge, 6: jet cavitation device, 7: water tank, 8: filters, 9: switch valves).

Table 7. Nozzle structure parameters.

Code	Inlet Diameter (mm)	Outlet Diameter (mm)	Chamber Length (mm)	Diameter (mm)
#1	2.5	3	8.8	16
#2	3	3.6	12	16

3. Results and Discussion

3.1. Main Effect Analysis

Figure 5 shows the main effect of each design parameter of the SOCJN on the response cavitation number and the VOF [23]. It can be seen from Figure 5 that the effect of inlet pressure and C_{DD2} on the response variables, including the VOF and the average cavitation number, is negligible as the factor level rises. The increase in C_{LD} would lead to a plummet in the VOF and an upsurge in the average cavitation number.

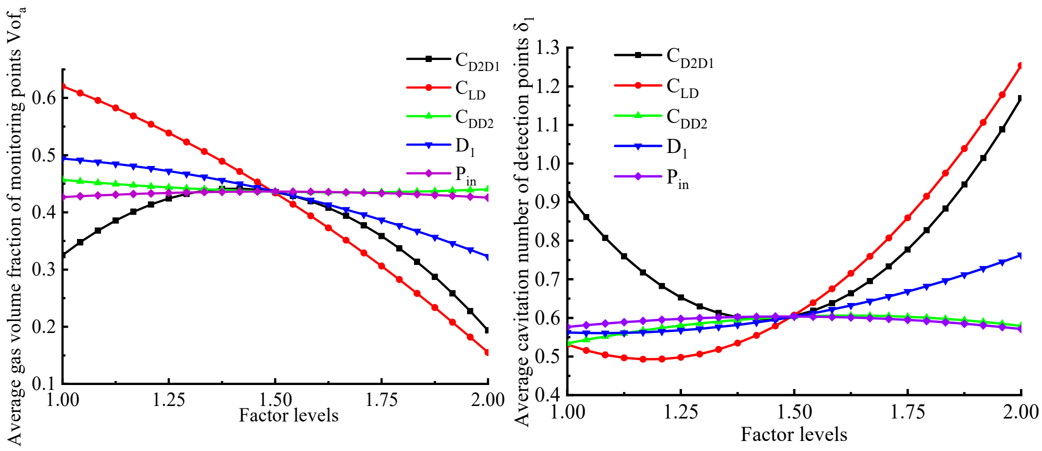

Figure 5. Main effect diagram.

With the increase in C_{D21}, the VOF falls after rising while the average cavitation number rises after falling, reaching the extreme point at the position of $C_{D21} = 1.50$. The increase in the inlet diameter D_1 will lead to a fall in the VOF and a rise in the average cavitation number; but, the influence is not as large as that of C_{LD} and C_{D21} on the response variables.

3.2. Analysis of Interaction Effect

Figures 6 and 7 show the interaction effect of each design parameter of the SOCJN on the response cavitation number and VOF [24]. It can be seen from the figures that C_{D21}, the ratio of the nozzle outlet diameter to the inlet diameter, has a significant interaction with the high and low points of the inlet diameter D_1. In addition, with the rise in C_{D21}, the average cavitation number at the high point of D_1 gradually increases and the VOF gradually decreases. The average cavitation number at the low point of D_1 rises after falling and the VOF falls after rising. C_{LD}, the ratio of the chamber length to its diameter, has a significant interaction with D_1.

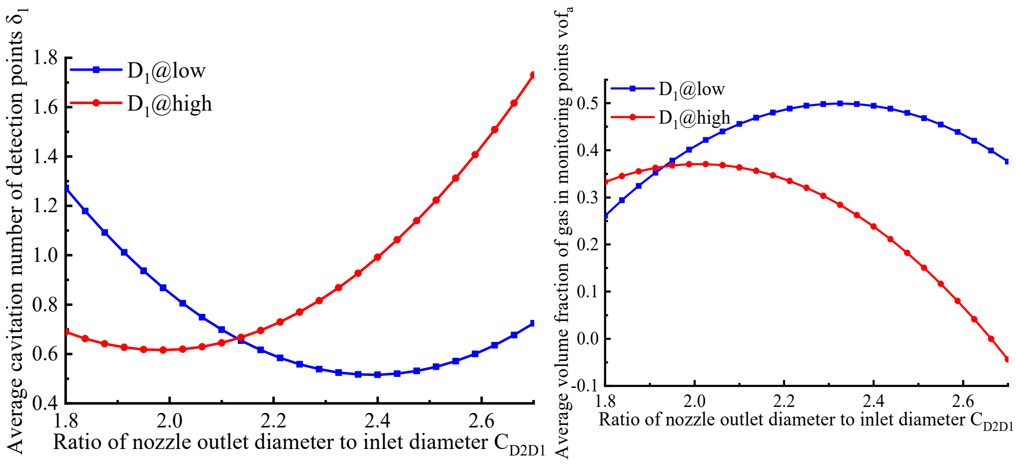

Figure 6. Interaction between C_{D21} and D_1.

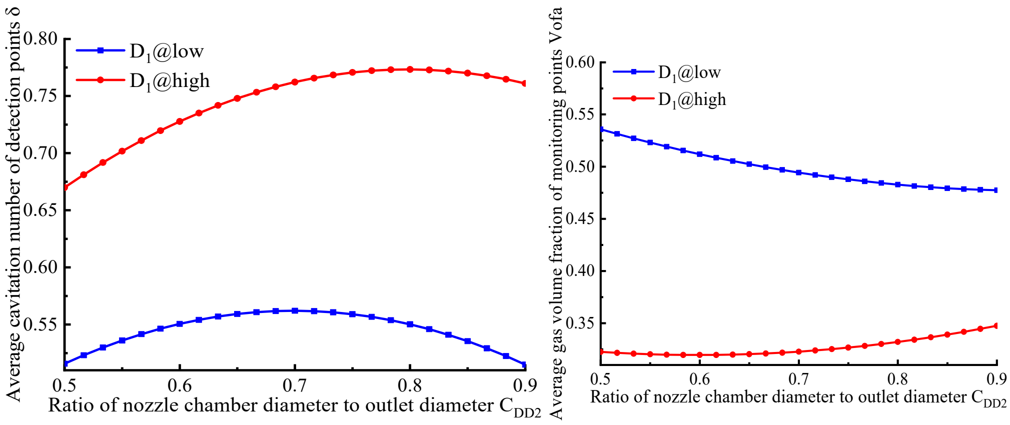

Figure 7. Interaction between C_{DD2} and D_1.

With the rise in C_{LD}, the average cavitation number at the high point of D_1 gradually increases and the VOF gradually decreases. The average cavitation number at the low point of D_1 rises after falling, with the inflection point appearing at $C_{LD} = 6$; but, the VOF keeps on falling. There is a less significant interaction between C_{DD2}, the ratio of chamber diameter to the outlet diameter, and D_1.

3.3. Pareto Plot and Correlation Analysis

Figure 8 shows the correlation diagram of the effect of each design parameter of the SOCJN on the response cavitation number and the VOF [25]. It can be seen from Figure 8 that the change in the nozzle inlet pressure pin basically has no effect on the average cavitation number and VOF. They are positively correlated with C_{LD}, with a correlation degree of around 0.6. D_1 is also positively correlated with them; but, the correlation is not as strong as that of C_{LD}. C_{D21} and C_{DD2} are also positively correlated; but, the correlation is weaker. The contribution rate of each design parameter of the SOCJN to the cavitation number σ and the VOF is shown in the Pareto diagram, in which the blue bar represents the positive effect and the red represents the negative. Figure 8 shows the design parameters of the nozzle. The second-order term and interaction term of the design parameters have opposite contribution rates to the cavitation number and VOF, which is inconsistent with the actual situation, indicating that it is infeasible to judge whether cavitation occurs and determine the cavitation degree with the cavitation number. The VOF is more reliable.

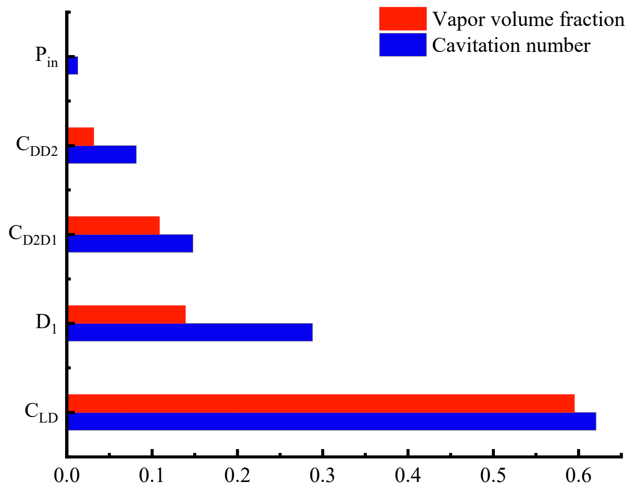

Figure 8. Correlation diagram.

It can be seen from the Pareto diagram of the VOF in Figure 9 that the dimensionless parameters of C_{D21}, C_{LD}, and C_{DD2} and the inlet diameter D_1 of the nozzle are all negatively correlated with the VOF; the dimensionless parameter C_{LD} has the largest contribution rate, followed by C_{D21} and C_{DD2}. C_{LD} is the ratio of the chamber length L to the chamber diameter D of the nozzle; so, the smaller the value, the better the cavitation performance of the nozzle.

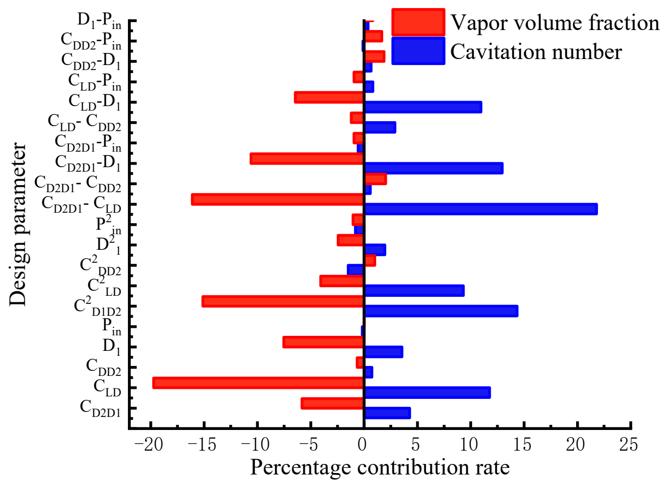

Figure 9. Pareto graphs.

3.4. Mathematical Model

According to the optimization model and approximate model, 501 iterative calculations are carried out using the ISIGHT software; all feasible solution sets are shown in Figure 10. All points in Figure 10 are feasible solutions for calculations. All of the points in the green circle are combined as the Pareto frontier and the optimal solution can be selected flexibly according to weight values. In this paper, the Pareto point solution is taken as the final result. One set of optimized data is selected for simulation and the simulated VOF distribution cloud map of the model before and after optimization is shown in Figure 9.

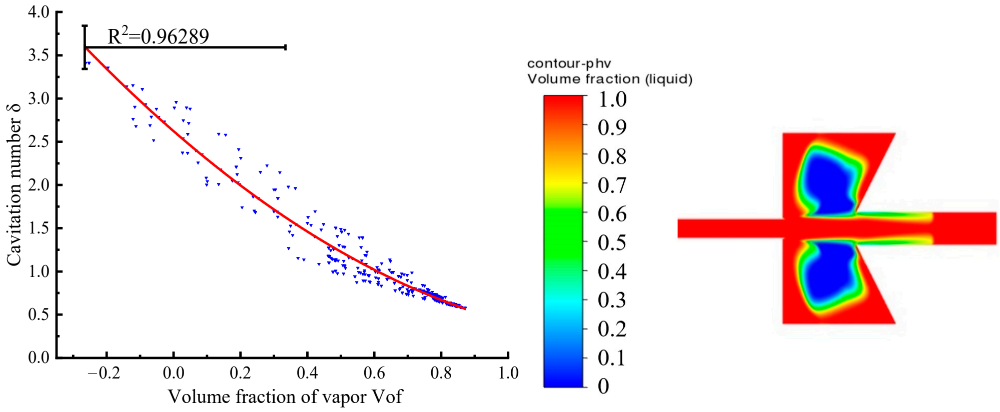

Figure 10. Pareto solution set and effect contour of one group after simulation optimization.

According to the attached table, since the inlet diameter determines the pressure and velocity levels, the cavitation performance weakens with the increase of the outlet diameter, which may be caused by the hindering effect of the nozzle outlet on the jets. Therefore, a suitable outlet diameter is conducive to reducing the energy loss. When the inlet diameter is 4.7, the outlet of the nozzle can better accept the energy provided by its inlet so that the energy loss is reduced and the cavitation performance is better. Hence, the proportioning relationship between the inlet and outlet of the nozzle is also very important. The pulse occurs when the inlet diameter of the SOCJN is 4.2 mm, 4.6 mm, or 4.9 mm and it becomes the most obvious when the diameter is 4.7 mm. Therefore, the parameter ratio of D_2/D_1 being between 2.2 and 2.67 is an optimal range and the best result happens when D_2/D_1 = 2.6. This is found by observing the changes in the chamber that show that the larger the chamber diameter, the larger the low-pressure range; the chamber diameter plays a critical role in deciding whether the vortex ring structure in the chamber is conducive to outputting effective kinetic energy and generating cavitation pockets that can change periodically.

The output of the nozzle outlet energy is also affected by the outlet and the chamber diameter. The optimization results demonstrate that the cavitation being performed is optimal when the ratio of chamber length to chamber diameter equals 0.63. The good cavitation performance of the nozzle is related to not only the high-speed jets at its inlet but also the pulse frequency. At a certain frequency, the uneven energy output of the pulsed jets will cause pressure oscillations in the chamber; but, the continuous alternating stress greatly improves the effect of cavitation. The cavitation performance is the best when the ratio of chamber length to chamber diameter is around 6.8 and the inlet pressure is around 4.8 MPa. Under these conditions, the VOF and cavitation number reach 0.6 and 0.5, respectively, proving that cavitation occurred and has an obvious performance.

3.5. Experimental Verification

An aluminum plate sample is placed squarely facing the SOCJN for a continuous 20 min lashing. Then, the pump is turned off to take out the sample. The obtained cavitation effect is shown in Figure 11. As shown in Figure 11, the results of the impact test by the nozzle indicate that the No. 3 nozzle has a relatively obvious impact range, with impacting marks that tend to be deeper from the center to the periphery. The No. 1 nozzle is the optimized nozzle and its impacting marks are smaller and shallower than those of the No. 2 and No. 3 nozzles. Although it causes severe erosion in the center area, the No.2 nozzle causes smaller impacting marks on the periphery, which also proves that the structural parameters of the No. 3 nozzle are a better group in the process of simulation. Adjusted on the basis of the optimal parameters, the No. 3 nozzle has a better impact than the No.

1 and No.2 nozzles. Based on the impact test, the SOCJN has an outstanding cavitation performance, with the capability to cause relatively vigorous cavitation. The feasibility of the SOCJN for refractory industrial wastewater treatment has been confirmed from the perspective of cavitation.

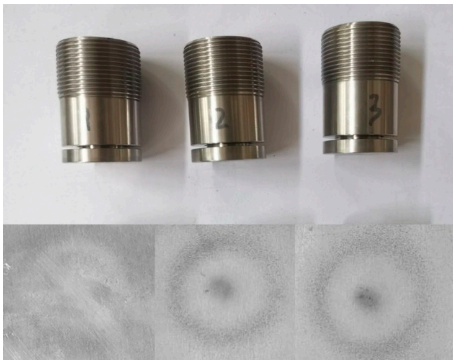

Figure 11. Impact test results with three groups of nozzles.

4. Conclusions

In this paper, the structure of the SOCJN is optimized by the optimizing Latin method and response surface method. The main conclusions are as follows:

(1) The self-oscillating pulsed jet from the SOCJN has the best cavitation performance at the monitoring point when the diameter of the upper nozzle D_L = 4.7 mm, the ratio of the upper diameter of the nozzle to the lower one D_1/D_2 = 2.6, the ratio of the cavity length to the cavity diameter L/D = 0.63, and the convergence angle of collision wall α = 120°, all of which are optimal structural parameters;

(2) When the structural parameters of the nozzle remain unchanged, the velocity at the outlet has a linear relationship with the initial working pressure and the cavitation performance increases with the rise in the initial pressure. When the initial pressure is greater than the threshold value, the cavitation performance begins to deteriorate. When the structural parameters of the nozzle are optimal structural parameters, the cavitation performance is the best at the initial pressure of about 4.8 Mpa;

(3) The fitting effect of the response surface approximation model is better than other approximate models. It finds that the second-order response surface approximate model is suitable for the SOCJN. There is an error smaller than 8% between the approximate model results and calculated results of the nozzle response, indicating that the former has high accuracy and the analysis results are reliable. The experimental results verify the reliability of this optimized design scheme.

In this paper, taking the vapor volume fraction as the research objective, a variety of design methods are used to optimize the design of the SOCJN. The relationship between the external geometric parameters of the nozzle and the vapor volume fraction is established and the comparison and verification are made with the experimental results, which provide a theoretical basis for the engineering application of the SOCJN.

Author Contributions: T.W.: Conceptualization; Data collection; Writing the original draft. G.L.: data collection; Writing original draft. M.S.: Writing original draft (Supporting), review and editing. X.W. and Y.Z.: Conceptualization (supporting); writing; review and editing. W.X.: Supervision, review and editing. F.Z.: Data collection, review and editing. All authors have read and agreed to the published version of the manuscript.

Funding: This research was supported by the Key projects of the joint fund of the National Natural Science Foundation of China [U20A20292]; Technology Support Plan (Research on Key Industrial Technologies) (TG202251).

Data Availability Statement: Not applicable.

Conflicts of Interest: The authors declare no conflict of interest.

Nomenclature

D_1	Nozzle inlet diameter (mm)
L	Nozzle chamber length (mm)
α	Collision wall convergence angle (°)
VOF	Vapor volume fraction (%)
P_{in}	Nozzle inlet pressure (Pa)
SS	Sum of squares of mean deviations
F	Statistic values
D_2	Nozzle outlet diameter (mm)
D	Chamber diameter (mm)
VOFa	Average vapor volume fraction at monitoring points (%)
C_{nm}	n/m, Dimensionless (n, m = D_1, D_2, L, D)
DF	Freedom
δ	Cavitation number
P	Inspection level
D_1@high	The high point of D_1
D_1@low	The low point of D_1

Appendix A

Table A1. Optimized Latin square test results of the SOCJN.

	C_{D21}	C_{LD}	C_{DD2}	D_1	P_{in}	VOFa	δ_1
1	2.6092	5.252	0.621	4.7899	1,537,815.126	0.3725	0.7155
2	1.9059	5.874	0.5235	4.6218	3,991,596.639	0.44015	0.5469
3	2.1176	6.714	0.5874	4.7227	1,235,294.118	0.17295	1.0468
4	1.9664	6.143	0.6681	4.958	2,042,016.807	0.3559	0.6988
5	2.6319	5.42	0.7992	4.9328	4,193,277.311	0.3014	0.7681
6	2.1328	5.891	0.6714	4.0336	3,823,529.412	0.5284	0.5174
7	2.6546	5.437	0.7118	4.3445	1,638,655.462	0.51678	0.5269
8	1.8832	5.555	0.7521	4.5798	1,134,453.782	0.3759	0.7607
9	2.1782	5.588	0.5269	4.4538	2,613,445.378	0.5735	0.4089
10	2.2311	5.773	0.7017	4.6303	2,176,470.588	0.4725	0.5337
11	2.5034	6.076	0.5639	4.084	4,495,798.319	0.4199	0.7091
12	2.0496	5.958	0.8227	4.2185	4,831,932.773	0.4983	0.4922
13	2.0874	6.479	0.6546	4.437	2,949,579.832	0.3717	0.7483
14	2.337	5.605	0.8664	4.7059	3,151,260.504	0.4623	0.5720
15	1.9134	6.21	0.8496	4.8403	2,714,285.714	0.3907	0.6127
16	2.4807	5.101	0.7891	4.5042	4,462,184.874	0.6453	0.3377
17	1.8227	6.261	0.7723	4.1933	3,285,714.286	0.2797	1.0732
18	2.4277	6.782	0.7824	4.7311	4,663,865.546	0.0363	2.1018
19	2.5714	6.16	0.658	4.6134	1,268,907.563	0.0933	1.1695
20	2.0042	5.168	0.6815	4.8992	1,873,949.58	0.5758	0.4661
21	2.1706	6.395	0.8966	4.563	3,924,369.748	0.2718	0.8439
22	2.4655	5.118	0.6479	4.5294	3,016,806.723	0.63028	0.3542
23	2.5941	5.134	0.7689	4.0924	3,588,235.294	0.6668	0.3299
24	1.9891	6.849	0.863	4.3782	2,546,218.487	0.3283	1.0248
25	1.9361	6.244	0.8395	4.1176	1,504,201.681	0.3210	0.7472
26	2.6924	5.807	0.7857	4.4202	3,352,941.176	0.4831	0.6291
27	2.5487	5.992	0.6916	4.6807	4,731,092.437	0.2242	0.9001
28	1.8303	5.79	0.6849	4.5966	2,915,966.387	0.3360	0.7479
29	2.6697	5.739	0.6445	4.0252	2,882,352.941	0.4456	0.5737
30	2.3824	5.151	0.7387	4.9496	2,680,672.269	0.5272	0.4808

References

1. Safikhani, H.; Abbassi, A.; Khalkhali, A.; Kalteh, M. Multi objective optimization of nanofluid flow in flat tubes using CFD, artificial neural networks and genetic algorithms. *Adv. Powder Technol.* **2014**, *25*, 1608–1617. [CrossRef]
2. Gogate, P.R.; Thanekar, P.D.; Oke, A.P. Strategies to improve biological oxidation of real wastewater using cavitation-based pre-treatment approaches. *Ultrason. Sonochem.* **2020**, *64*, 105016. [CrossRef] [PubMed]
3. Ge, M.; Sun, C.; Zhang, G.; Coutier-Delgosha, O.; Fan, D. Combined suppression effects on hydrodynamic cavitation performance in Venturi-type reactor for process intensification. *Ultrason. Sonochem.* **2022**, *86*, 106035. [CrossRef] [PubMed]
4. Ge, M.; Zhang, G.; Petkovšek, M.; Long, K.; Coutier-Delgosha, O. Intensity and regimes changing of hydrodynamic cavitation considering temperature effects. *J. Clean. Prod.* **2022**, *338*, 130470. [CrossRef]
5. Pappaterra, M.; Xu, P.; van der Meer, W.; Faria, J.A.; Rivas, D.F. Cavitation intensifying bags improve ultrasonic advanced oxidation with Pd/Al2O3 catalyst. *Ultrason. Sonochem.* **2021**, *70*, 105324. [CrossRef]
6. Askarniya, Z.; Sun, X.; Wang, Z.; Boczkaj, G. Cavitation-based technologies for pretreatment and processing of food wastes: Major applications and mechanisms—A review. *Chem. Eng. J.* **2023**, *454*, 140388. [CrossRef]
7. Hu, J.; Yuan, M.; Feng, G.; Wang, X.; Li, D. Experimental investigation on the cavitation modulation mechanism in submerged self-sustained oscillating jets. *Ocean Eng.* **2023**, *274*, 114108. [CrossRef]
8. Wang, B.; Su, H.; Zhang, B. Hydrodynamic cavitation as a promising route for wastewater treatment—A review. *Chem. Eng. J.* **2021**, *412*, 128685. [CrossRef]
9. Zhang, X.; Li, X.; Nie, S.; Wang, L.; Dong, J. Study on velocity and pressure characteristics of self-excited oscillating nozzle. *J. Braz. Soc. Mech. Sci. Eng.* **2021**, *43*, 5. [CrossRef]
10. Gensheng, L.; Debin, Z.; Zhongwei, H. Self-Excited Oscillating Water Injection: Mechanisms and Experiments. *Pet. Sci. Technol.* **2003**, *21*, 145–155.
11. Zhu, F.; Wang, Z.; Lv, M. Multiobjective optimization of precision forging process parameters based on response surface method. *Adv. Mater. Sci. Eng.* **2015**, *7*, 730–893. [CrossRef]
12. An, W.; Wei, J.; Lu, X.; Dai, J.S.; Li, Y. Geometric Design-based Dimensional Synthesis of a Novel Metamorphic Multi-Fingered Hand with Maximal Workspace. *Chin. J. Mech. Eng.* **2021**, *34*, 41. [CrossRef]
13. Li, G.; Shen, Z.; Zhou, C.; Dengbi, Z.H.; Can, Y. An experimental study on impact pressure characteristics of self-resonant cavitating jets. *J. Hydrodyn. A* **2003**, *5*, 570–575.
14. Liu, Y.; Sun, L.J.; Li, Z.; Wang, Y.X. Numerical Simulation of Cavitation Jet in a Double Chamber Self-Excited Oscillation Pulse Nozzle. *Ship Electron. Eng.* **2020**, *40*, 95–98.
15. Qi, M.; Wang, L.F.; Chen, Q.G.; Zhao, J.L.; Ju, Y.H.; Fu, Q.Q. Numerical simulation of cavitating jet in dual chamber self-oscillation pulse nozzle. *J. Drain. Irrig. Mach. Eng. (JDIME)* **2020**, *38*, 457–461. (In Chinese)
16. Yuan, X.; Wang, N.; Wang, W.; Zhang, L.; Zhu, Y. Nozzle resonance mechanism and cooperative optimization of self-excited oscillating pulse cavitation jet. *Trans. Can. Soc. Mech. Eng.* **2023**, *27*, 74–78. [CrossRef]
17. Wang, T.Y.; Li, X.; Zhang, K.M.; Huang, Y.C.; Yang, F.; Huang, C.D. Numerical simulation of flow field characteristics of Helmholtz self-vibrating cavitation device. *J. Guangxi Univ. Sci. Technol.* **2021**, *32*, 1–11.
18. Juraeva, M.; Song, D.J.; Kang, D.J. Computational optimization approach to design a water-jet nozzle for a water-jet loom using the design of experiment method. *J. Mech. Sci. Technol.* **2019**, *33*, 631–637. [CrossRef]
19. Raut-Jadhav, S.; Saini, D.; Sonawane, S.; Pandit, A. Effect of process intensifying parameters on the hydrodynamic cavitation based degradation of commercial pesticide (methomyl) in the aqueous solution. *Ultrason. Sonochem.* **2016**, *28*, 283–293. [CrossRef]
20. Jyoti, K.; Pandit, A. Water disinfection by acoustic and hydrodynamic cavitation. *Biochem. Eng. J.* **2001**, *7*, 201–212. [CrossRef]
21. Deng, L.F.; Long, Y.; Cheng, H.Y.; Ji, B. Some notes on numerical investigation of three cavitation models through a verification and validation procedure. *J. Hydrodyn.* **2023**, *35*, 185–190. [CrossRef]
22. Zheng, S.; Nishimura, S.-I.; Shuku, T.; Shibata, T.; Tateishi, T. Risk evaluation for earth-fill dams due to heavy rains by response surface method. *Georisk Assess. Manag. Risk Eng. Syst. Geohazards* **2023**, *17*, 572–585. [CrossRef]
23. Zhang, X.; Shi, X.; Liu, Y.; Liu, X.; Ma, S. A General Framework for Identifying Hierarchical Interactions and Its Application to Genomics Data. *J. Comput. Graph. Stat.* **2022**, *32*, 873–883. [CrossRef]
24. Wu, S.N.; Xu, Y.Q.; Zhang, Q.Z.; Ma, S.G. Gene-environment interaction analysis via deep learning. *Genet. Epidemiol.* **2023**, *47*, 261–286. [CrossRef]
25. Nagar, D.; Ramu, P.; Deb, K. Visualization and analysis of Pareto-optimal fronts using interpretable self-organizing map (iSOM). *Swarm Evol. Comput.* **2023**, *76*, 101202. [CrossRef]